

nate. The resulting images represented two mutually orthogonal dimensions in the cortex, horizontal and vertical, and clearly demonstrated that the distribution of functionally defined cells across the cortex is not only nonuniform but also highly structured. On the basis of these images, we propose a structural model of local organization of directionally tuned cells.

Methods

Neurophysiological Data Set. Experimental data used in this work came from previous extracellular single cell recordings (17). Monkeys reached out to push lighted buttons located in 3D space. Movements were free and unconstrained and were made from the same starting position in eight distinct directions that covered the whole 3D directional continuum at approximately equal angular intervals. Microelectrode penetrations were made in the proximal arm area of the motor cortex. Although certain functional cell properties may change in the anteroposterior dimension (23), no changes have been observed with respect to the motor properties of cells, including their directional tuning during movement. While monkeys performed the task, (i) the spike activity of single cells was recorded, and (ii) the microelectrode position, at which an individual cell was isolated along the depth of a penetration, was registered. The directionally tuned cells were identified, and their PD vectors were determined (17). The data used in the present study included 463 directionally tuned cells recorded in 79 penetrations made in four hemispheres of two monkeys. All cells were well isolated, as judged by two experimenters.

Method for Detection of Functionally Defined Local Cortical Modules.

In this analysis, we considered the PD vector of a directionally tuned cell as a characteristic feature of its function, whereas the position of recording microelectrode at which the cell was isolated provided information about its location in the cortex. We introduce the notion of the local functional neuron density field, $h(x, \psi)$, as a quantity that characterizes the functional neighborhood of a typical cell recorded in a penetration. It is expressed in terms of the density of neurons whose PDs deviate by a given angle ψ and are recorded at a distance x along the penetration axis, from the PD and the position of a reference cell isolated in the same penetration, respectively.

Specifically, $h(x, \psi)$ is computed as follows. Consider a particular penetration in which n directionally tuned cells were recorded. Let us place the x axis of a rectangular lattice along the penetration line, with the lattice origin $(0, 0)$ at a neuron i ($i = 1, 2, \dots, n$). The coordinate x thus indicates the position of a given neuron recorded in the penetration with respect to the particular neuron i at the origin of the lattice. The second axis of the lattice, orthogonal to x , represents the functional “distance” of a given neuron from the reference neuron i , which is specified by the angle, ψ , between their PD vectors ($0 \leq \psi \leq \pi$). Each lattice cell is a box with sides Δx and $\Delta \psi$ in x and ψ dimensions, respectively. The contribution of cell i into the local functional neuron density field at (x, ψ) is given by $n_i(x, \psi) / (\Delta x \cdot \Delta \psi)$, where $n_i(x, \psi)$ is the number of cells inside a box with the coordinates (x, ψ) . Visiting all boxes that fall within the penetration boundaries, which are determined by the positions of the most superficial and deep neurons recorded in the penetration, one can obtain the total contribution of the particular neuron i into the local density field. We then reposition the lattice origin on the next neuron in the sample and repeat the whole procedure. After considering every neuron $i = 1, 2, \dots, n$ recorded in the penetration, we finally obtain $h(x, \psi)$ as a sum of the contributions to the field from all neurons in the sample: $h(x, \psi) = 1/N(x) \sum_{i=1}^n n_i(x, \psi) / (\Delta x \cdot \Delta \psi)$, where $N(x)$ is the number of cases (i.e., positions of the lattice with a particular cell at its origin) in which boxes with the coordinate x were inside the penetration boundaries. Such a definition of $h(x, \psi)$ with the

normalization factor $N(x) \leq n$ takes into account so-called boundary or end effects, which are due to the finite length L of the sampled depth of the cortex in an individual penetration.

Finally, after computing $h(x, \psi)$ for each penetration included in a particular set Ω , we determine the average functional neuron density field $g(x, \psi)$ for this set by averaging across all local density fields $h(x, \psi)$ obtained from individual penetrations in Ω : $g(x, \psi) = \langle h(x, \psi) \rangle_{\Omega}$. Note that the integral $g(x) = \int_0^{\pi} d\psi g(x, \psi)$ is the 1D analog of the neuron density field (or the neuron density correlation function) considered in ref. 22 and represents the density of recorded cells, irrespective of their particular functional property, in the vicinity of a typical neuron. Integrating $g(x, \psi)$ for the second time, now over x , we obtain the average neuron density ρ_0 , which is the number of isolated cells per unit length in a typical penetration: $\rho_0 = 1/2L \int_{-\bar{L}}^{\bar{L}} dx \int_0^{\pi} d\psi g(x, \psi)$, where \bar{L} is the averaging length.

The reasonable values for lattice parameters Δx and $\Delta \psi$ are dictated by the precision of measurements of the corresponding variables in neurophysiological experiments. These parameters were varied in the range of $22.5^\circ < \Delta \psi < 45^\circ$, $60 \mu\text{m} < \Delta x < 90 \mu\text{m}$, and the images were robust to these variations. Images represented in the present paper were obtained with these parameters fixed at $\Delta x = 75 \mu\text{m}$ and $\Delta \psi = 30^\circ$.

Monte Carlo (MC) Simulations. Once the functional neuron density field $g(x, \psi)$ is calculated from a neurophysiological data set Ω , a key question is whether the observed pattern $g(x, \psi)$ is due to local fluctuations in a uniformly random distribution of directionally tuned cell positions and PDs, or whether $g(x, \psi)$ indeed reveals a nontrivial functionally defined cortical module. We addressed this question by performing MC simulations and assessing the magnitude of statistical noise in the local density fields obtained from randomly generated penetration samples, as follows.

For a given penetration of length L , taken from an experimental set Ω comprising penetrations with the average neuron density ρ_0 , we create a corresponding random sample consisting of n “neurons” generated from a Poisson distribution with mean density ρ_0 , on an interval of length L . The PD vector of each such neuron is independent of PD vectors of other neurons in the sample and is randomly drawn from the uniform distribution of unit vectors in a 3D space. After creating such samples for each penetration in the set Ω , we calculate the functional neuron density field $g_r(x, \psi)$ produced by this particular realization of samples from a universe in which the PDs and positions of neurons are completely at random, whereas the average neuron density and the lengths of individual samples are the same as those in the actual penetrations. This whole procedure is repeated N_{MC} times, and the mean, $\bar{g}_r(x, \psi)$, and the standard deviation, $\sigma_g(x, \psi)$ of the functional neuron density fields produced by completely random samples are calculated. Finally, we express the functional neuron density field $g(x, \psi)$ obtained from actual penetrations in the following normalized form: $\rho(x, \psi) = (g(x, \psi) - \bar{g}_r(x, \psi)) / \sigma_g(x, \psi)$.

In the course of these simulations, we also count the number of cases, $n_{\text{MC}}(x, \psi)$, in which $g_r(x, \psi) < g(x, \psi)$. We then estimate the probability $p(x, \psi)$ that the functional neuron density field $g_r(x, \psi)$ produced by a random sample is less than the density field $g(x, \psi)$ generated from actual penetrations as the ratio: $p(x, \psi) = n_{\text{MC}}(x, \psi) / N_{\text{MC}}$. The probability $p(x, \psi)$ is used to estimate the statistical significance of the observed increase in the functional neuron density ($\rho(x, \psi) > 0$) or conversely the decrease ($\rho(x, \psi) < 0$) with respect to the mean density $\bar{g}_r(x, \psi)$ generated from random samples.

In standard simulations, $N_{\text{MC}} = 10^5$. MC iterations were performed, although we also conducted several simulations in which $N_{\text{MC}} = 10^6$. In these cases, the results were practically identical to those obtained with the smaller number of iterations.

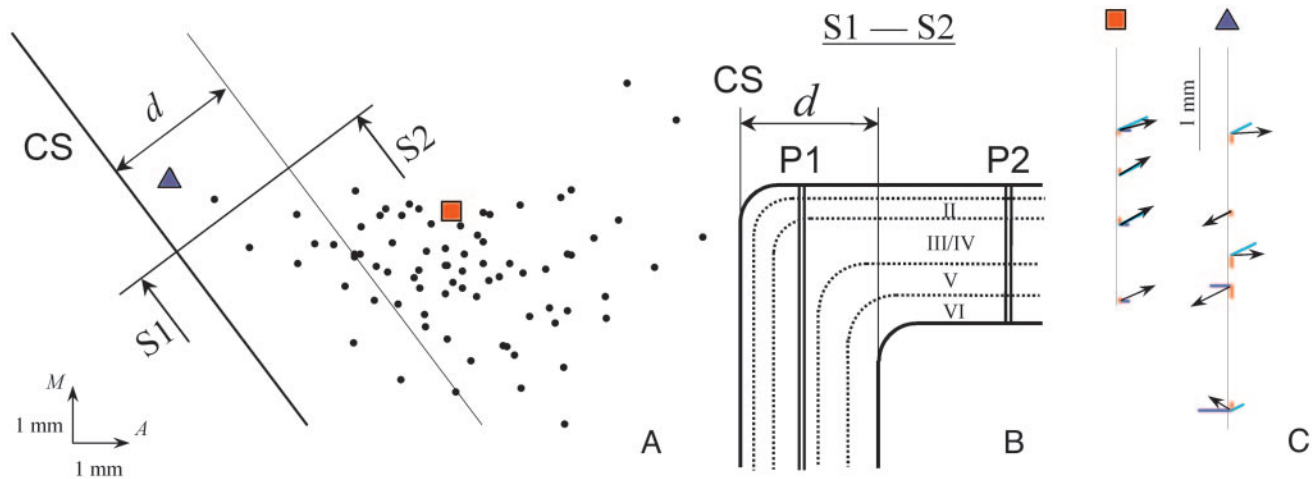


Fig. 1. (A) Surface view showing the location of entry points with respect to the CS of 79 penetrations used in the present study. For graphical purposes, data from four hemispheres are transformed and plotted on an outline of a right hemisphere (see figure 6 in ref. 17). The transformation is invariant with respect to the distance between a particular entry point and the CS. The continuous line parallel to, and at a distance d from, the CS represents a borderline that demarcates the cortical surface into two regions (see text). The imaginary sections S1–S2 orthogonal to the CS is shown in B. A, anterior; M, medial. (B) Section view of the cortical depth in a plane orthogonal to the CS (S1–S2, in A). Dotted curves schematically represent the cortical laminae. Double lines illustrate the orientations of two imaginary penetrations P1 and P2 made nearby and farther away from the CS, respectively. The bisecting borderline is shown here in a similar fashion as in A. II–VI cortical layers. (C) Examples of two penetrations analogous to P1 and P2. The entry points of the penetrations are color-shape coded in A and C. The PDs of directionally tuned cells isolated along the penetrations are shown as arrows, with the corresponding direction cosines in color. It can be seen that PDs were very similar along the penetration resembling P2 (red square), whereas they differed appreciably in the penetration resembling P1 (blue triangle). The average angle between PDs of all cell pairs was 19° for the former and 96° for the latter penetration.

Finally, a different MC procedure, in which cell positions were not changed, whereas PDs were drawn from the neurophysiological data set Ω , produced similar results.

Results

Quantification of Cell Function and Spatial Location from Experiments.

Single cell recordings in the brain of behaving animals may simultaneously provide two distinct types of information: (i) functional (i.e., specific activity of cells during a particular behavioral task) and (ii) spatial (i.e., location of the recorded cells in the cortex). In the present study, we analyzed data from 463 directionally tuned cells recorded in the motor cortex of monkeys while they performed reaching movements in a 3D space (17). In the functional domain, we used the PD vector as a quantitative measure of the directional tuning, whereas in the spatial domain, we used the coordinates of isolated cell positions along the direction of the microelectrode penetration. The number of cells n recorded in a single penetration was usually small ($2 \leq n \leq 15$). Therefore, in the framework of our approach, an accurate consideration of the functional modularization of the cortex requires an averaging across a set of coherent penetrations, i.e., penetrations that sampled the vicinity of a given cortical region in similar directions.

Regarding the penetrations relevant to the present study, the surface coordinates of their entry points were known, but the precise orientation of these penetrations with respect to the cortical laminae was not determined. It is important to notice, however, that the approximate orientation of a given penetration can be determined on the basis of the location of the entry point of the penetration on the cortical surface. This is explained in Fig. 1. Fig. 1A illustrates schematically a surface view of the recorded cortical area showing the location of entry points of penetrations used in this study with respect to the central sulcus (CS). In contrast, Fig. 1B illustrates a section view of the cortical depth in a plane orthogonal to the CS and shows schematically the convoluted structure of the cortex in the region of the CS. One can appreciate from the diagrams shown in Fig. 1 that penetrations made perpendicular to the cortical surface and at

positions farther away from the CS (penetration P2, Fig. 1B) are nearly orthogonal to the cortical laminae. In contrast, similar penetrations at locations near the CS (penetration P1, Fig. 1B) are nearly parallel to the laminae. The cortical surface, therefore, can be roughly divided into two distinct regions that are distinguished by a particular orientation of penetrations, parallel or orthogonal, with respect to the cortical laminae. The imaginary borderline that separates these two regions is approximately parallel to, and lies at some distance d from, the outline of the CS on the cortical surface (see Fig. 1). The approximate value of d is determined by the thickness of the cortex in the anterior bank of the CS.

Taking into account this consideration, for a given position d of the borderline described above, we partitioned the complete set of penetrations, Ω_Σ , from the experimental database into two nonoverlapping subsets $\Omega_\perp(d)$ and $\Omega_\parallel(d)$ such that $\Omega_\perp(d) \cup \Omega_\parallel(d) = \Omega_\Sigma$. The subset $\Omega_\parallel(d)$ comprised all penetrations whose entry points were proximal to the CS and were confined to the cortical surface demarcated by the CS and the borderline. In a further analysis, the orientations of penetrations in $\Omega_\parallel(d)$ were considered as nearly parallel to the cortical laminae. Conversely, the subset $\Omega_\perp(d)$ included all penetrations made at distal positions from the CS, beyond the borderline. The orientations of penetrations in $\Omega_\perp(d)$ were treated as nearly perpendicular to the cortical laminae.

Functional Neuron Density Fields. We calculated the normalized forms of functional neuron density fields $\rho_\parallel(x, \psi)$ and $\rho_\perp(x, \psi)$ (see *Methods*) for sets $\Omega_\parallel(d)$ and $\Omega_\perp(d)$, respectively. The parameter d defining the position of imaginary borderline was varied in the range of 2.0–5.0 mm, which is comparable with the depth of the monkey motor cortex (25). It is noteworthy that by moving the borderline closer to the CS (smaller d), one reduces the likelihood of contamination of $\Omega_\parallel(d)$ with penetrations that are not parallel to the cortical laminae (see Fig. 1B). Conversely, by moving the borderline farther away from the CS (larger d), one reduces the likelihood of contamination of $\Omega_\perp(d)$ with penetrations that are not orthogonal to the laminae (see Fig. 1B).

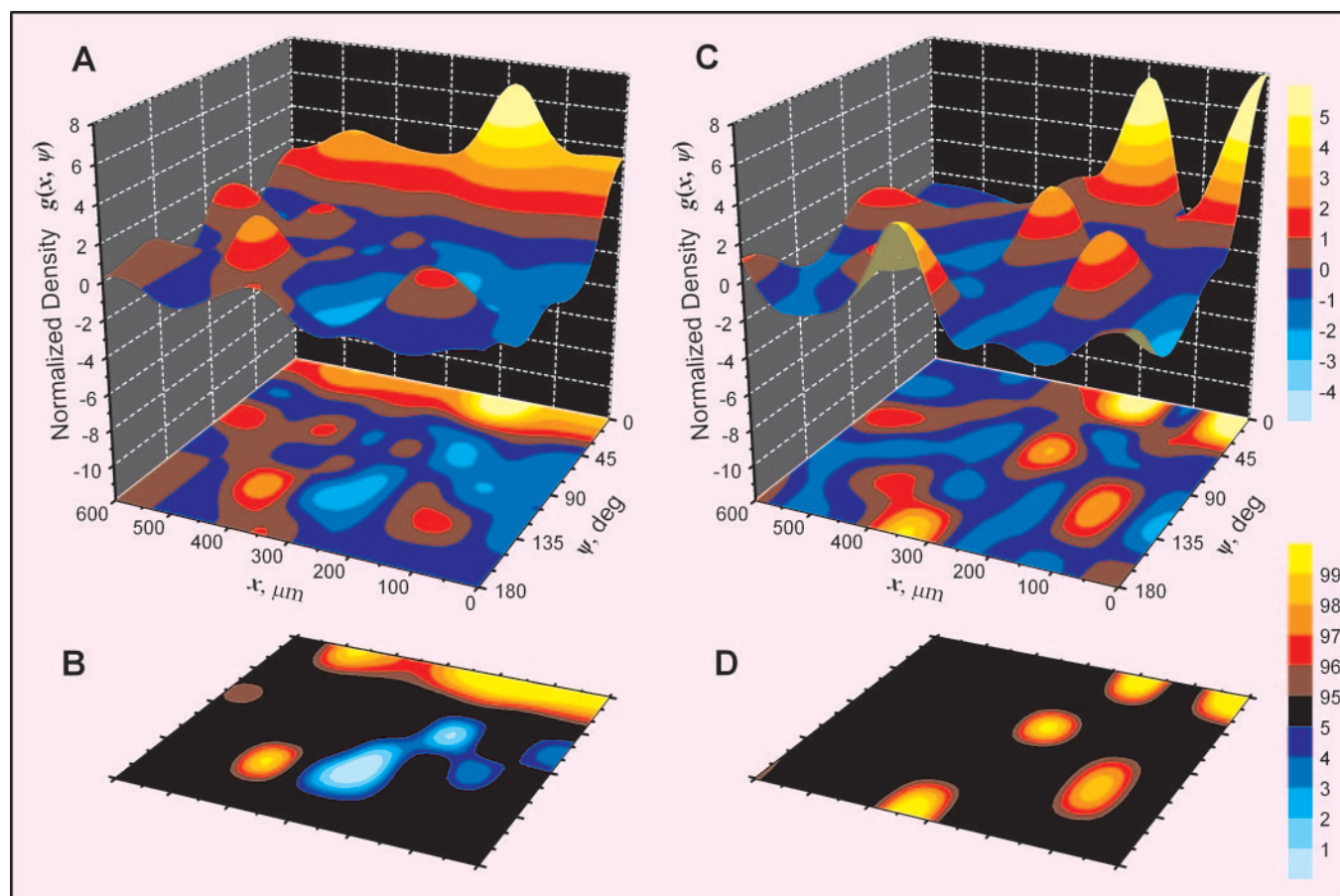


Fig. 2. Images representing functional neuron density fields computed for two mutually orthogonal dimensions. (A and C) The functional neighborhood of a typical cell, which is located in the origin (0, 0) of an image, is shown as a 3D landscape with the corresponding 2D contour map of the density $\rho(x, \psi)$ of cells recorded at a spatial distance x and at a functional distance ψ (the angular deviation of cell PD from the reference cell). $\rho(x, \psi)$ is normalized with respect to, and is expressed in the standard deviation units of, the density obtained from uniformly random samples (see *Methods*). The color scale shows color-coded values of $\rho(x, \psi)$ in the images. (B and D) The density field $\rho(x, \psi)$ and its corresponding probability map $p(x, \psi)$ computed for a uniformly random sample is less than the density field generated from actual penetrations is shown as a 2D contour map. The color scale shows color-coded values of $p(x, \psi)$ in the percentile units. In the red-yellow (blue-cyan) region the probability that a random sample will have the density above (below) the observed value is $<5\%$, whereas in the black regions this probability is $>5\%$. (A and B) The density field $\rho_{\perp}(x, \psi)$ and its corresponding probability map $p(x, \psi)$ computed for the set Ω_{\perp} that includes penetrations treated as nearly perpendicular to the cortical laminae. (C and D) The density field $\rho_{\parallel}(x, \psi)$ and its corresponding probability map $p(x, \psi)$ computed for the set Ω_{\parallel} that includes penetrations treated as nearly parallel to the cortical laminae. For graphical purposes, the computed images defined on the binned discrete (x, ψ) space were interpolated by a continuous smooth surface by using tensor-product B-spline interpolant (IMSL Math Library, Visual Numerics, Houston). Visual inspection revealed that in the region of negative x ($-600 \mu\text{m} < x$), the plots for $\rho(x, \psi)$ and $p(x, \psi)$ are practically indistinguishable from the region of positive x ($x < +600 \mu\text{m}$) (they would be strictly symmetric if the end effects were not accounted for). Therefore, only regions $x > 0$ are shown.

However, these qualitative improvements in the composition of penetrations making up sets Ω_{\parallel} or Ω_{\perp} are at the expense of quantitative losses in the number of penetrations contributing to these sets (see Fig. 1A). Accordingly, the density fields $\rho_{\parallel}(x, \psi)$ and $\rho_{\perp}(x, \psi)$ showed some dependence on a specific value of parameter d . However, the fields did change consistently as a function of d ; importantly, the major features of individual images $\rho_{\parallel}(x, \psi)$ and $\rho_{\perp}(x, \psi)$ (pointed out below) were present within the examined range of d . This observation suggests the robustness of the penetration partitioning procedure.

The examples for $\rho_{\parallel}(x, \psi)$ and $\rho_{\perp}(x, \psi)$ shown in Fig. 2 were computed for the values of $d = 2.5$ mm and $d = 4.0$ mm, respectively. The sets Ω_{\parallel} and Ω_{\perp} produced by these values provide a reasonable compromise between the quality and quantity of penetrations that contribute to the corresponding images. The resulting set Ω_{\perp} included 151 cells recorded in 31 penetrations in which the average number of neurons recorded per unit length $\rho_0 = 4.8$ cells/mm. The set Ω_{\parallel} comprised 72 cells isolated in 13 penetrations with average neuron density $\rho_0 = 2.3$

cells per mm. It should be noted that if the underlying penetrations are partitioned properly, the lengths of penetrations in Ω_{\perp} should not exceed the depth of the monkey motor cortex [≈ 2.5 mm (24)]; in contrast, penetrations in Ω_{\parallel} could be much longer (see Fig. 1B). Indeed, the vast majority of the penetrations in Ω_{\perp} were shorter than 1.5 mm, whereas the longest one was 2.1 mm. Conversely, most of the penetrations in Ω_{\parallel} were longer than 2.0 mm, the longest one reaching 5.6 mm. It is noteworthy that, due to the layered structure of the cortex, there is no reason to expect that the linear density of neurons should be isotropic. The observed difference in ρ_0 is, therefore, another indication that the partitioning of penetrations into the sets Ω_{\parallel} and Ω_{\perp} was done appropriately. Nevertheless, to assure the robustness of our approach with respect to the variation in ρ_0 we down-sampled the original penetrations in Ω_{\perp} to yield its corresponding ρ_0 comparable to the one in the set Ω_{\parallel} . This down-sampled data set yielded very similar results as those obtained from the whole data set, shown below.

Fig. 2A shows a 3D color-coded landscape and its correspond-

ing 2D contour plot of the functional neuron density field $\rho_{\perp}(x, \psi)$ in the vertical dimension (see above). The axis x represents the cell position along the penetration relative to a reference neuron at the origin (0,0) of the image, and, for this set of penetrations, is assumed to be perpendicular to the cortical laminae. The axis ψ represents the angular deviation of cell PD vector from the PD vector of the reference cell and is interpreted as a “distance” from the reference neuron in the functional domain. A positive (or negative) value of $\rho_{\perp}(x, \psi)$ indicates that the density of neurons obtained from experimental penetrations in Ω_{\perp} is larger (or, conversely, smaller) than the density that one would expect from uniformly random penetration samples (see *Methods*). The magnitude of $\rho_{\perp}(x, \psi)$ is expressed in units of standard deviation for the random samples. Fig. 2*B* shows a 2D contour map of the probability $p(x, \psi)$ that $\rho_{\perp}(x, \psi) < 0$ (see *Methods*). Note that $1 - p(x, \psi)$ is, conversely, the probability that $\rho_{\perp}(x, \psi) > 0$. The color scale is chosen such that in a red-yellow (blue-cyan) region, the probability that a random sample has the density above (below) the observed value is $< 5\%$, whereas in the black regions this probability is $> 5\%$.

Fig. 2*A* and *B* indicates that the local distribution of directionally tuned cells in the vertical dimension is not only nonuniform but also highly structured. Particularly, cells with similar PDs ($0^{\circ} < \psi < 30^{\circ}$) form a continuous densely-packed neuronal domain extending across cortical laminae as far as $500 \mu\text{m}$ (red band in the interval $[0, 525] \mu\text{m}$, Fig. 2*A* and *B*) with a peak density (yellow region, Fig. 2*A*) at $\approx 200 \mu\text{m}$. Inside of this domain, there is a deficit of cells with PDs between 60° and 150° (blue region in the interval $[150, 300] \mu\text{m}$) and an excess of cells with nearly opposite PDs ($\psi \approx 135^{\circ}, x \approx 400 \mu\text{m}$). Thus the image representing the vertical dimension suggests that cells with similar and nearly opposite PDs participate in the formation of an ordered local structure.

The functional neuron density field $\rho_{\parallel}(x, \psi)$ in the horizontal dimension and its probability map $p(x, \psi)$ are depicted in Fig. 2*C* and *D*, respectively, in a fashion similar to Fig. 2*A* and *B*. Note that the x axis is now parallel to the cortical laminae. It is seen that the local distribution of functionally defined cells in this dimension is also structured, although the observed pattern differs from that shown in Fig. 2*A*. Specifically, neurons with similar PDs do not segregate into a large continuous domain, but instead, they form isolated relatively narrow ($75\text{-}\mu\text{m}$ -wide) regions with a spacing of $\approx 200 \mu\text{m}$. These regions of cells with similar PDs are interleaved with high-density regions of cells with PDs ranging from nearly orthogonal to nearly opposite directions ($90^{\circ} < \psi < 150^{\circ}, x \approx 100 \mu\text{m}$, and $60^{\circ} < \psi < 90^{\circ}, x \approx 250 \mu\text{m}$). Moreover, a distinct region of cells with opposite PDs located further away from the image origin ($150^{\circ} < \psi < 180^{\circ}, x \approx 350 \mu\text{m}$) suggests that in the horizontal dimension, a local order in the arrangement of directionally tuned cells can be present at distances up to $350 \mu\text{m}$.

Finally, when the functional density field $g(x, \psi)$ was collapsed (integrated) along the functional axis ψ , the resulting density $g(x)$ was almost flat for both horizontal and vertical dimensions (data not shown).

Structural Model. Taking into consideration the fact that images shown in Fig. 2 come from two mutually orthogonal dimensions, we propose the following model of cortical organization of directionally tuned cells.

The presence of a strong relatively long-range ($0\text{--}525 \mu\text{m}$) spatial correlation between neurons with similar PDs in the vertical dimension (Fig. 2*A* and *B*), together with the presence of short-range ($0\text{--}75 \mu\text{m}$) correlation in the horizontal dimension (Fig. 2*C* and *D*), suggest that neurons with similar PDs segregate into vertically oriented column-shape functional structures of $\approx 50\text{--}100 \mu\text{m}$ wide and at least $500 \mu\text{m}$ high. In such a column, which can be conceived as representing a particular PD,

similarly tuned cells are distributed in a continuous fashion, although they tend to be separated by a distance of $\approx 200 \mu\text{m}$ along the column axis (see Fig. 2*A*). Within this module, there is also an order in the arrangement of cells with nearly opposite PDs. The spacing between a pair of cells with opposite PDs is $\approx 400 \mu\text{m}$ along the long axis of the column.

Spatial correlations observed in Fig. 2*C* and *D* suggest that columns aggregate across the horizontal dimension in a structure of a higher order (we shall call it the “secondary structure”) with a characteristic size of at least $350 \mu\text{m}$. It comprises columns representing similar PDs, with an approximate spacing $200 \mu\text{m}$, interleaved with columns representing nearly orthogonal PDs. Because PD vectors are 3D it should be noted that vectors orthogonal to a given PD may come from a continuum of directions in 3D space rather than from a single direction. Finally, the long-range ($350 \mu\text{m}$) correlation between cells with opposite PDs (Fig. 2*C* and *D*) suggests that within the secondary structure, columns representing opposite PDs are $\approx 350 \mu\text{m}$ apart.

Discussion

Past decades have witnessed the ascension to prominence of circuit-oriented concepts in cortical processing (25–28). In a current theory of the neocortex (1, 29, 30), a key hypothesis is that local microcircuits, which are embedded in minicolumns, are elemental processing units: they are repeated many times in each cortical area and have similar vertically oriented patterns of intrinsic connections (27). A significant contribution to the formulation of this hypothesis was the discovery of functional columniation of cells in several cortical areas including somatosensory, visual, and auditory. In the present work, we addressed the issue of whether a modularization of functionally defined

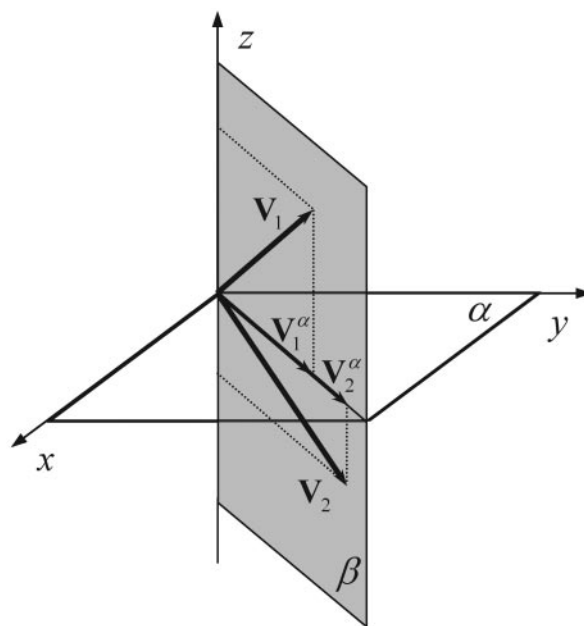


Fig. 3. Illustration of the ambiguity concerning cell PDs determined from movements in 2D space. Consider a cell with its actual PD vector V_1 defined in 3D movement space (x, y, z) . If movements from which PDs are determined were constrained to the 2D plane α , then this cell would have an apparent PD vector collinear to the projection, V_1^{α} , of its actual PD vector on the plane α . Because the projection of any vector in the semiplane β orthogonal to the plane α is collinear to V_1^{α} , the actual PD cannot be recovered from such experiments. Moreover, a pair of cells with different PD vectors V_1 and V_2 in the plane β would have “similar” PDs determined from movements in the 2D plane α .

cells may also exist in the motor cortex. We investigated this problem by applying a method that detected local correlations between the functional properties of a cell and its position. Both of these quantities were measured in the course of single cell recordings from the motor cortex of monkeys while they moved their arm toward targets in 3D space. The neurophysiological recordings allow direct measurements of the functional properties of individual cells, but this comes at the expense of substantial losses in the accuracy of data in the spatial domain. Unlike morphological methods in which 2D coordinates of cells in slices are measured under a microscope, the coordinates of neurons isolated in electrophysiological recordings are determined by the position of the microelectrode tip along the penetration axis; therefore, the recorded coordinates are essentially 1D. In addition, due to the large sampling radius ($\gg 1 \mu\text{m}$) of the microelectrode tip, the spatial resolution in electrophysiological recordings is much lower than the resolution provided by optical microscopes ($< 1 \mu\text{m}$).

Because the directional tuning is a prominent feature of motor cortical cells (16, 31–34), we chose the PD vector as the functional quantitative measure. In this context, it is important to note that, for any PD mapping study, it is imperative that the PDs of cells be determined from movements made in 3D space. If movements in 2D space are used instead, this could lead to erroneous mapping, because a particular PD in 2D space can reflect an infinite number of PDs in 3D space, as illustrated in Fig. 3.

- Mountcastle, V. B. (1998) *Perceptual Neuroscience: The Cerebral Cortex* (Harvard Univ. Press, Cambridge, MA).
- Mountcastle, V. B. (1997) *Brain* **120**, 701–722.
- Mountcastle, V. B. (1957) *J. Neurophysiol.* **20**, 408–434.
- Powell, T. P. S. & Mountcastle, V. B. (1959) *Bull. Johns Hopkins Hosp.* **105**, 133–162.
- Hubel, D. & Wiesel, T. N. (1962) *J. Physiol.* **160**, 106–154.
- Hubel, D. & Wiesel, T. N. (1974) *J. Comp. Neurol.* **158**, 267–293.
- Blasdel, G. G. & Salama, G. (1986) *Nature* **321**, 579–585.
- Grinvald, A., Lieke, E., Frostig, R. P., Gilbert, C. & Wiesel, T. (1986) *Nature* **324**, 351–354.
- Blasdel, G. G. (1992) *J. Neurosci.* **12**, 3139–3161.
- Maldonado, P. E., Gödecke, I., Gray, C. M. & Bonhoeffer, T. (1997) *Nature* **276**, 1551–1555.
- Merzenich, M. M. & Brugge, J. F. (1973) *Brain Res.* **50**, 275–296.
- Ahissar, M., Ahissar, E., Bergman, H. & Vaadia, E. (1992) *J. Neurophysiol.* **67**, 203–215.
- Morel, A., Garraghty, P. E. & Kass, J. H. (1993) *J. Comp. Neurol.* **335**, 437–459.
- Asanuma, H. (1975) *Physiol. Rev.* **55**, 143–156.
- Kwan, H. C., MacKay, W. A., Murphy, J. T. & Wong, Y. C. (1978) *J. Neurophysiol.* **41**, 1120–1131.
- Georgopoulos, A. P., Kalaska, J. F., Caminiti, R. & Massey, J. T. (1982) *J. Neurosci.* **2**, 1527–1537.
- Schwartz, A. B., Kettner, R. E. & Georgopoulos, A. P. (1988) *J. Neurosci.* **8**, 2913–2927.
- Schwartz, A. B. & Moran, D. W. (2000) *Eur. J. Neurosci.* **12**, 1851–1856.
- Johnson, M. T. V., Mason, C. R. & Ebner, T. J. (2001) *Curr. Opin. Neurobiol.* **11**, 684–688.
- Georgopoulos, A. P., Kalaska, J. F., Crutcher, M. D., Caminiti, R. & Massey, J. T. (1984) in *Dynamic Aspects of Neocortical Function*, eds. Edelman, G. M., Gall, W. E. & Cowan, W. M. (Wiley, New York), pp. 501–524.
- Ben-Shaul, Y., Stark, E., Asher, I., Drori, R., Nadasy, Z. & Abeles, M. (2003) *J. Neurophysiol.* **89**, 1136–1142.
- Buldirev, S. V., Cruz, L., Gomez-Isla, T., Gomez-Tortosa, E., Havlin, S., Le, R., Stanley, H. E., Urbanc, B. & Hyman, B. T. (2000) *Proc. Natl. Acad. Sci. USA* **97**, 5039–5043.
- Johnson, P. B., Ferraina, S., Bianchi, L. & Caminiti, R. (1996) *Cereb. Cortex* **6**, 102–119.
- Rockel, A. J., Hiorns, R. W. & Powell, T. P. S. (1980) *Brain* **103**, 221–244.
- Szentagothai, J. (1976) *Exp. Brain Res. Suppl.* **1**, 282–287.
- Creutzfeldt, O. D. (1977) *Naturwissenschaften* **64**, 507–518.
- Mountcastle, V. B. (1978) in *The Mindful Brain*, eds. Edelman, G. M. & Mountcastle, V. B. (MIT Press, Cambridge, MA), pp. 7–50.
- Douglas, R. J. & Martin, K. A. C. (1991) *Trends Neurosci.* **14**, 286–293.
- Jones, E. G. (2000) *Proc. Natl. Acad. Sci. USA* **97**, 5019–5021.
- Mountcastle, V. B. (2003) *Cereb. Cortex* **13**, 2–4.
- Kalaska, J. F., Cohen, D. A. D., Hyde, M. L. & Prud'homme, M. (1989) *J. Neurosci.* **9**, 2080–2102.
- Caminiti, R., Johnson, P. B. & Urbano, A. (1990) *J. Neurosci.* **10**, 2039–2058.
- Georgopoulos, A. P., Ashe, J., Smyrnis, N. & Taira, M. (1992) *Science* **256**, 1692–1695.
- Lin, L. D., Murray, G. M. & Sessle, B. J. (1994) *J. Neurophysiol.* **71**, 2391–2400.
- Bauer, R., Dow, B. M., Snyder, A. Z. & Vautin R. (1983) *Exp. Brain Res.* **50**, 133–145.

This work was supported by U.S. Public Health Service Grant NS17413, the U.S. Department of Veterans Affairs, and the American Legion Brain Sciences Chair.